ELSEVIER

Solid State Ionics 81 (1995) 97–109

SOLID STATE IONICS

Oxygen transport through $La_{1-x}Sr_xFeO_{3-\delta}$ membranes. I. Permeation in air/He gradients

J.E. ten Elshof *, H.J.M. Bouwmeester, H. Verweij

University of Twente, Department of Chemical Technology, Laboratory of Inorganic Materials Science, P.O. Box 217, 7500 AE Enschede, The Netherlands

Received 22 March 1995; accepted for publication 26 July 1995

Abstract

Oxygen permeation measurements in air/He gradients were performed on dense $La_{1-x}Sr_xFeO_{3-\delta}$ membranes in the composition range $x = 0.1$–0.4 and temperature range 1123–1323 K. Pretreatment of the lower oxygen partial pressure side of the membranes in a CO-containing atmosphere for several hours at 1273 K led to higher oxygen fluxes, which were in the range of 0.1–4.5 mmol m^{-2} s^{-1}. After treatment, the observed oxygen fluxes could be described in terms of bulk diffusion-limited permeation behaviour. Experimental evidence for a bulk-diffusion controlled flux was found from thickness dependence measurements on membranes with thicknesses between 0.5 mm and 2.0 mm. Model calculations, based on Wagner theory in conjunction with data of oxygen nonstoichiometry and vacancy diffusion coefficients from literature, were performed. The experimental flux values deviated from the model calculations with factors up to 2.5. Adjustment of the value of the vacancy diffusion coefficient led to good agreement between the experimental data and the model calculations. The calculated vacancy diffusion coefficients D_V^0 were virtually independent of composition and were found to be in the range 5.3–9.3×10^{-6} cm^2 s^{-1}.

Keywords: Oxygen permeation; Mixed conductor; Lanthanum strontium iron oxide; Perovskite; Bulk diffusion

1. Introduction

Doping of oxygen-conducting ceramics with multivalent cations can lead to the simultaneous occurrence of ionic and electronic conductivity. In recent years the study of such mixed conductors has received considerable attention, since they hold promise for use as membranes for air separation or as a combined oxygen supplying membrane and catalyst in membrane reactors [1–3]. Provided that the membrane is fully dense, it is impermeable to all gases except oxygen. Attention was initially paid to yttria- and calcia-stabilized zirconia (YSZ and CSZ, respectively) based systems [4–6]. More recently, mixed ionic–electronic conducting oxides of the fluorite and perovskite structure have drawn interest [7–10].

Oxygen fluxes through perovskite membranes were first reported by Teraoka et al. [8,11], who showed preliminary results for $La_{1-x}A_x$-$Co_{1-y}M_yO_{3-\delta}$ membranes (A = Ca, Sr, Ba; M = Co, Fe, Cu, Ni). The oxygen flux was found to be

* Corresponding author. Fax: +31-53-339546; E-mail: j.e.tenelshof@ct.utwente.nl.

SSDI 0167-2738(95)00177-8

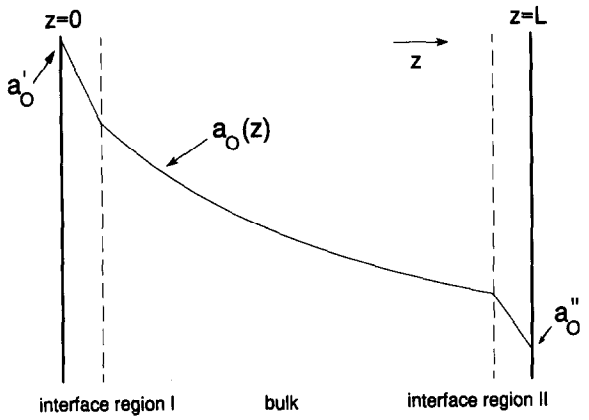

Fig. 1. Schematic oxygen activity profile inside a membrane placed in a gradient. The gas phase activities are denoted by a'_{O_2} and a''_{O_2}.

roughly proportional to the ionic conductivity [11]. The results obtained suggest a relationship between the oxygen semi-permeability and the reducibility of the perovskite [12]. Currently, the research efforts mainly focus on earth-alkaline doped cobaltites $La_{1-x}A_xCoO_{3-\delta}$ (A = Ca, Sr, Ba) which combine high oxygen semi-permeability [9–11] in the temperature range of 1000–1200 K, and chemical stability above 10^{-4} bar O_2 at elevated temperatures [13].

The oxygen activity in a membrane of thickness L, placed in an oxygen partial pressure gradient, is schematically shown in Fig. 1 as a function of z ($0 \leqslant z \leqslant L$). Oxygen activity drops will generally occur in both interface regions and the bulk of the material. It is therefore of particular interest for practical applications to know whether the oxygen flux is limited by bulk diffusion or by a surface exchange process for a certain composition. In the former case, the oxygen flux will be inversely proportional to the membrane thickness. Higher permeation rates can then be achieved by reducing the thickness.

In the latter case, beneficial effects can only be expected from surface enlargement and modification. A characteristic thickness L_c indicating the membrane thickness at which the oxygen flux is equally limited by bulk diffusion and surface exchange kinetics, has been derived on theoretical grounds [14], provided that the electronic transference number is close to unity:

$$L_c = \frac{D_O^*}{k}. \tag{1}$$

Here D_O^* is the tracer diffusion coefficient ($cm^2\ s^{-1}$) and k is the surface exchange coefficient ($cm\ s^{-1}$). If $L < L_c$, the oxygen flux will be limited predominantly by the surface exchange kinetics. It should be noted that the characteristic thickness is not an intrinsic material property, but depends on oxygen partial pressure and temperature.

Oxygen diffusion through the bulk may be modelled using Wagner theory [15], provided that sufficient literature data are available on the defect chemistry or conductivity parameters of the material under consideration. The $La_{1-x}Sr_xFeO_{3-\delta}$ solid solution system ($0 \leqslant x \leqslant 1$) has been studied extensively, which makes it an attractive material for modelling purposes. Dissolution of SrO in $LaFeO_{3-\delta}$ enhances the formation of oxygen vacancies. The oxygen nonstoichiometry parameter δ depends on oxygen partial pressure and temperature and can, in principle, take any value between 0 and 0.5. From thermogravimetric measurements, Mizusaki et al. [16] were able to describe the defect chemistry for $x = 0$–0.6 in the temperature range 873–1473 K and oxygen partial pressure range 10^{-20}–1 bar, assuming a random distribution of oxygen vacancies [16]. Adopting Kröger–Vink notation [17] the defect model consists of an oxidation reaction:

$$2Fe_{Fe}^{\times} + V_O^{\cdot\cdot} + \tfrac{1}{2}O_2(g) \rightleftharpoons 2Fe_{Fe}^{\cdot} + O_O^{\times} \tag{2}$$

and a charge disproportionation reaction:

$$2Fe_{Fe}^{\times} \rightleftharpoons Fe_{Fe}^{\cdot} + Fe_{Fe}^{\prime}. \tag{3}$$

The corresponding equilibrium constants are essentially independent of the level of nonstoichiometry, which might indicate that the defects in $La_{1-x}Sr_xFeO_{3-\delta}$ are randomly distributed on their lattice sites.

Comparison between the experimental results and statistical thermodynamic calculations later confirmed that the defect chemistry of $La_{1-x}Sr_xFeO_{3-\delta}$ can be properly described by the random distribution approximation [18]. Since according to this model all oxygen vacancies exist as point defects, it implies

Table 1
Estimated characteristic thickness L_c as function of composition. $T = 1273$ K and $P_{O_2} = 0.065$ bar. Data taken from Refs. [28,29]

x	L_c (mm)
0	$3 \cdot 10^{-4}$
0.1	0.06
0.25	0.3
0.4	0.45

that all oxygen vacancies can contribute to the transport of oxygen. Study of the local structure of several perovskite systems by electron diffraction, HR-TEM and Mössbauer spectroscopy has shown that, depending on the degree of nonstoichiometry, a variety of phases with the general formula $A_mM_mO_{3m-1}$ can exist [19]. These are structurally located between the brownmillerite structure ($AMO_{2.5}$, $m = 2$) and the perovskite structure (AMO_3, $m = \infty$). Such phases have also been discovered for $SrFeO_{3-\delta}$ [20] and for $La_{1/3}Sr_{2/3}FeO_{3-\delta}$ [21] and their general structure can be thought of as consisting of $(m-1)$ layers in which Fe is octahedrally coordinated by oxygen, separated by a layer in which iron occupies tetrahedrally coordinated sites. In the latter layer, all the oxygen vacancies are ordered along one of the cubic ⟨110⟩ directions. Within a single phase, microdomains with vacancy ordering in different directions may be intergrown [22,23] and the simultaneous existence of microdomains with different m values has also been observed [20,24]. In any case, these observations are not only in disagreement with the point defect model described above, it is also generally believed that ordered oxygen vacancies are immobile and will thus not contribute to oxygen transport. Alternative structural models have been proposed for $SrFeO_{2.75}$ [25,26] and for $La_{1/3}Sr_{2/3}FeO_{2.806}$ [21], in which layers of Fe in square pyramidal coordination are separated by two layers of Fe in octahedral coordination. In this structure, the oxygen vacancies would exist as point defects, though ordered. A similar model was proposed for $La_{0.5}Ba_{0.5}FeO_{2.75}$ [27] on the basis of electron diffraction experiments. However, in order to be consistent with the experimental results, it had to be assumed that the oxygen vacancies are disordered in the layers with five-fold coordination. Unfortunately, the structural studies are usually carried out at room temperature on quenched samples. It is well possible that some ordering phenomena originate from the cooling process instead of representing high temperature equilibrium structures. More research is required to study the evolution of these extended defects.

A study on the oxygen semi-permeability of 0.5–2 mm thick $La_{1-x}Sr_xFeO_{3-\delta}$ membranes ($x = 0.1$–0.4) in air/He gradients is reported in this paper. To determine the nature of the rate-limiting step in oxygen transport, a comparison will be made between fluxes calculated from Wagner theory, using data from literature, and the experimental results. The characteristic thicknesses L_c for compositions in the range $x = 0.1$–0.4 can be estimated from data obtained by Ishigaki et al. from $^{18}O/^{16}O$ isotope exchange experiments [28,29], as shown in Table 1. L_c increases with increasing Sr-concentration and it is seen that the transition from bulk to surface control occurs in the mm-range. In a forthcoming paper [30] we will report on the oxygen flux through $La_{1-x}Sr_xFeO_{3-\delta}$ membranes when placed in a large gradient, i.e. CO/CO_2.

Table 2
Thermodynamic quantities of oxidation and charge disproportionation reactions (2) and (3) as a function of composition. Data taken from Ref. [16]

x	ΔH_{ox} (kJ/mol)	ΔS_{ox} (J/mol K)	ΔH_i (kJ/mol)	ΔS_i (J/mol K)
0.1	−112	−67	159	11
0.25	−112	−75	179	33
0.4	−100	−67	123	−5

2. Theory

2.1. Nonstoichiometry

The equilibrium constants corresponding to reactions (2) and (3) are

$$K_{ox} = \frac{[O_O^\times][Fe_{Fe}^\times]^2}{[V_O^{\cdot\cdot}][Fe_{Fe}^{\cdot}]^2 P_{O_2}^{1/2}} = \exp\left[-\frac{(\Delta H_m - T\Delta S_m)}{RT}\right] \quad (4)$$

and

$$K_i = \frac{[Fe'_{Fe}][Fe_{Fe}^{\cdot}]}{[Fe_{Fe}^\times]^2} = \exp\left[-\frac{(\Delta H_i - T\Delta S_i)}{RT}\right]. \quad (5)$$

From thermogravimetric experiments, the values of the thermodynamic quantities were determined by Mizusaki et al. [16] The as-determined values are given in Table 2. Within experimental error, the thermodynamic quantities were found to be independent of composition for $x = 0.1$–0.6, with the exception of ΔH_i [18].

Taking into account the condition of charge neutrality

$$[Sr'_{La}] + [Fe'_{Fe}] = [Fe_{Fe}^{\cdot}] + 2[V_O^{\cdot\cdot}] \quad (6)$$

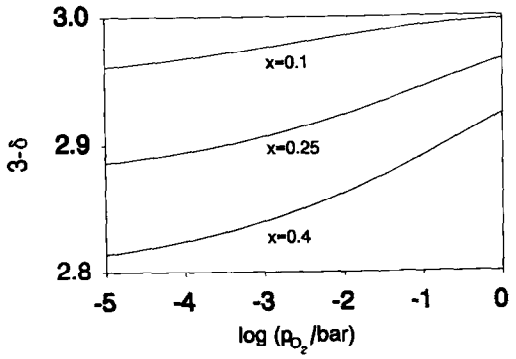

Fig. 2. Calculated nonstoichiometries of $La_{1-x}Sr_xFeO_{3-\delta}$ for $x = 0.1$–0.4 as a function of log P_{O_2} at 1273 K.

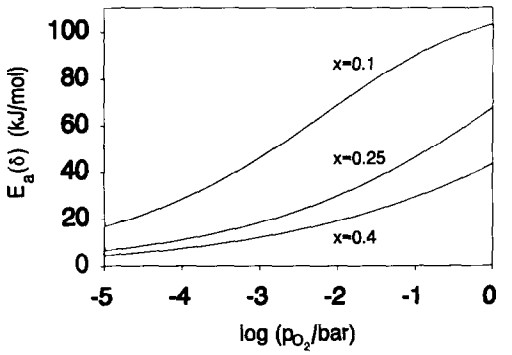

Fig. 3. Calculated activation energies for oxygen vacancy formation.

and the constraints given by Eqs. (7) and (8) due to the stoichiometry of the perovskite

$$[Fe_{Fe}^\times] + [Fe_{Fe}^{\cdot}] + [Fe'_{Fe}] = 1, \quad (7)$$

$$[O_O^\times] + [V_O^{\cdot\cdot}] = 3 \quad (8)$$

we finally have five equations. The Sr concentration $[Sr'_{La}]$ is given by the nominal A-site composition, thus $[Sr'_{La}] = x$. The degree of nonstoichiometry $[V_O^{\cdot\cdot}]$ will further be referred to as δ. With Eqs. (4)–(8) and the data from Table 2, the concentrations of all species can be calculated analytically as a function of P_{O_2} and T for a given composition. If we set the nonstoichiometry to a certain value δ at a given temperature T, we can combine Eqs. (5)–(7) to obtain a second-order polynomial expression for $[Fe_{Fe}^{\cdot}]$:

$$[Fe_{Fe}^{\cdot}]^2(4K_i - 1) + [Fe_{Fe}^{\cdot}] \times [-4K_i + (x - 2\delta)(1 - 4K_i)] + K_i[1 + 2(x - 2\delta) + (x - 2\delta)^2] = 0. \quad (9)$$

With the values of δ and $[Fe_{Fe}^{\cdot}]$, the calculation of the concentrations of the other charge-carrying species is trivial. Finally, the corresponding oxygen partial pressure P_{O_2} can be calculated from Eq. (4). Fig. 2 shows the calculated oxygen concentrations of these compositions as a function of P_{O_2} at 1273 K. In Fig. 3 the activation energies for oxygen vacancy formation are shown as a function of the oxygen partial pressure. It can be seen that the activation

energy depends strongly on both the oxygen partial pressure and the Sr-content.

2.2. Ionic conductivity

In Sr-doped ferrite perovskites the ionic conductivity is due to diffusion of oxygen anions. If the mobile ions move independently of another an analytical expression is given by the Nernst–Einstein relation

$$\sigma_{ion} = \sigma_{O^{2-}} = \frac{z_O^2 F^2 D_O c_O}{RTN_A} \tag{10}$$

with D_O and c_O the diffusion coefficient and the concentration of oxygen anions. z_O and N_A are the ionic charge of lattice oxygen and Avogadro's constant, respectively. Since the diffusion of oxygen anions is physically equal to the diffusion of oxygen vacancies in the opposite direction, the product $D_O c_O$ is related to the concentrations of oxygen vacancies c_V via

$$D_O c_O = D_V c_V, \tag{11}$$

D_V is the vacancy diffusion coefficient. In accordance with the point defect model described above, it is assumed here that singly- and non-ionized oxygen vacancies do not exist. Furthermore, it is assumed that all oxygen vacancies are mobile, i.e. no clustering of vacancies occurs. Then

$$\sigma_{ion} = \frac{4F^2 D_V c_V}{RTN_A} = \frac{4F^2 D_V \delta}{RTV_m}, \tag{12}$$

where V_m is the molar volume of the perovskite unit cell. Although V_m is dependent on temperature and oxygen partial pressure, no data are available, and therefore it is assumed constant here. In general, the vacancy diffusion coefficient will be slightly dependent on the oxygen nonstoichiometry [31]. Due to the perovskite stoichiometry, the factor $(1 - \delta/3)$ represents the fraction of sites in the oxygen sublattice to which an oxygen vacancy can jump. An expression for D_V may thus be written as

$$D_V = D_V^0\left(1 - \frac{\delta}{3}\right). \tag{13}$$

Using nonstoichiometry data [16], Ishigaki et al. [28,29] calculated oxygen vacancy diffusion coefficients D_V from experimentally determined tracer diffusion coefficients for $x = 0$, 0.1, 0.25 and 0.4, as well as the corresponding activation energies for $x = 0$, 0.1 and 0.25. The latter values were found to be in the range of 75–114 kJ/mole. From the tracer diffusion coefficients reported by Kim et al. [32] for $x = 0.4$ and $x = 0.6$ a similar activation energy can be calculated. It was suggested that the activation energy is virtually independent of the Sr content [29]. D_V^0 values used in this study were calculated from the results of Ishigaki et al. and are listed in Table 3.

2.3. Electronic conductivity

The electronic conductivity in $La_{1-x}Sr_xFeO_{3-\delta}$ is thought to occur via Fe^{n+}–O–$Fe^{(n+1)+}$ conduction pairs ($n = 2$, 3) [33]. Because of the simultaneous occurrence of Fe^{2+}, Fe^{3+} and Fe^{4+}, n-type and p-type conductivity coexist. An analytical expression for the electronic conductivity was given by Mizusaki et al. [34]:

$$\sigma_{el} = \sigma_e + \sigma_p = [Fe'_{Fe}]\frac{N_A}{V_m}e(1 - [Fe'_{Fe}])\mu_e + [Fe^{\cdot}_{Fe}]\frac{N_A}{V_m}e(1 - [Fe^{\cdot}_{Fe}])\mu_p, \tag{14}$$

where σ_e and σ_p are the electron and electron hole conductivity (S m^{-1}). μ_e and μ_p (m^2 V^{-1} s^{-1}) are the mobilities of electrons and electron holes, respec-

Table 3
Constants used in Eqs. (12)–(14). Data obtained from Refs. [16,28,29] (D_V^0), Ref. [35] (V_m) and Ref. [34] (μ_p and μ_e)

x	D_V^0 (10^{-6} cm^2 s^{-1}) ($T = 1273$ K)	V_m (cm^3 mol^{-1})	μ_p (cm^2 V^{-1} s^{-1})	μ_e (cm^2 V^{-1} s^{-1})
0.1	7.43	36.4	0.10	0.08
0.25	13.38	36.0	0.09	0.07
0.4	20.39	35.6	–	–

tively. The mobilities for $x = 0.1$ and $x = 0.25$ were determined from conductivity and Seebeck measurements [34] and are listed in Table 3.

2.4. Bulk diffusion and ambipolar conductivity

When an oxygen partial pressure gradient is applied across a dense membrane made of $La_{1-x}Sr_xFeO_{3-\delta}$ oxygen will diffuse from the high to the low partial pressure side. A joint flux of electrons or electron holes maintains local charge neutrality throughout the membrane. Assuming a bulk diffusion-controlled flux, the oxygen flux is expressed by [15]:

$$J_{O_2} = \frac{RT}{4^2F^2L}\int_{P''_{O_2}}^{P'_{O_2}} \sigma_{amb}(P_{O_2})\, d\ln P_{O_2}. \quad (15)$$

Here J_{O_2} is the oxygen permeation flux in mol m^{-2} s^{-1}, P'_{O_2} and P''_{O_2} are the oxygen partial pressures at opposite sides of the membrane and L is the membrane thickness (m). The ambipolar conductivity σ_{amb} (S m^{-1}) is defined by

$$\sigma_{amb} = \frac{\sigma_{ion}\sigma_{el}}{\sigma_{ion} + \sigma_{el}}. \quad (16)$$

σ_{ion} is the ionic conductivity (S m^{-1}) and σ_{el} the electronic conductivity (S m^{-1}). The ambipolar conductivity can also be written in an empirical form:

$$\sigma_{amb} = \sigma_0 P_{O_2}^{n(P_{O_2})}, \quad (17)$$

where σ_0 is a constant (S m^{-1}) and n is called the order of the ambipolar conductivity. The validity of Eq. (15) is limited to cases where the overall transport is limited by bulk diffusion. With the model described above, the ambipolar conductivity can be calculated analytically. The total oxygen flux in a given partial pressure gradient can then be obtained by numerical integration. An analytical solution to the Wagner equation has also been described [36], assuming a constant D_V and $\sigma_{amb} = \sigma_{ion}$. The former assumption may not hold when the level of Sr-doping is considerable, while the latter does not hold at low oxygen partial pressures, typically in the range of 10^{-5}–10^{-15} bar in the temperature region of interest.

Since the ambipolar conductivity is a function of the oxygen partial pressure, its order with respect to the oxygen partial pressure can be calculated from

$$n(P'_{O_2}) = \left(\frac{\partial \ln \sigma_{amb}(P'_{O_2})}{\partial \ln P'_{O_2}}\right) = \left(\frac{\partial}{\partial \ln P'_{O_2}} \ln\left(\frac{\partial J_{O_2}}{\partial \ln P'_{O_2}}\right)_{P''_{O_2}}\right). \quad (18)$$

If $\sigma_{el} \gg \sigma_{ion}$, then $\sigma_{amb} \approx \sigma_{ion}$. Substitution of Eq. (12) into Eq. (18) then yields

$$n(P'_{O_2}) \approx \left(\frac{\partial \ln \sigma_{ion}(P'_{O_2})}{\partial \ln P'_{O_2}}\right) = \left(\frac{\partial \ln D_V\delta}{\partial \ln P'_{O_2}}\right) \approx \left(\frac{\partial \ln \delta}{\partial \ln P'_{O_2}}\right). \quad (19)$$

Since D_V does not change strongly in comparison with δ, the value of $n(P'_{O_2})$ will be determined mainly by the change of oxygen nonstoichiometry δ with changing oxygen partial pressure. An average value of n over a limited partial pressure range can be obtained from

$$\langle n \rangle = \int_{P''_{O_2}}^{P'_{O_2}} n(P_{O_2})\, d\ln P_{O_2} \Big/ \int_{P''_{O_2}}^{P'_{O_2}} d\ln P_{O_2}. \quad (20)$$

3. Experimental

3.1. Membrane synthesis

Stoichiometric amounts of nitrate solutions of the constituent metals were mixed in Q_2-water. 1.5 mole of citric acid was added per mole of metal. The pH was kept below 2 using HNO_3. Water was evaporated until the liquid became viscous. The solution was then pyrolysed in a stove. The resulting powder was calcined at 1123–1150 K for 10 h and subsequently ball-milled with YSZ milling balls in acetone for three hours. Disks of 20 mm diameter were obtained by subsequent uniaxial pressing at 1.5 bar and isostatic pressing at 4000 bar. The disks were sintered at 1473 K for 18–24 h in stagnant air. Membranes of 12.0 mm diameter and 0.5–2 mm

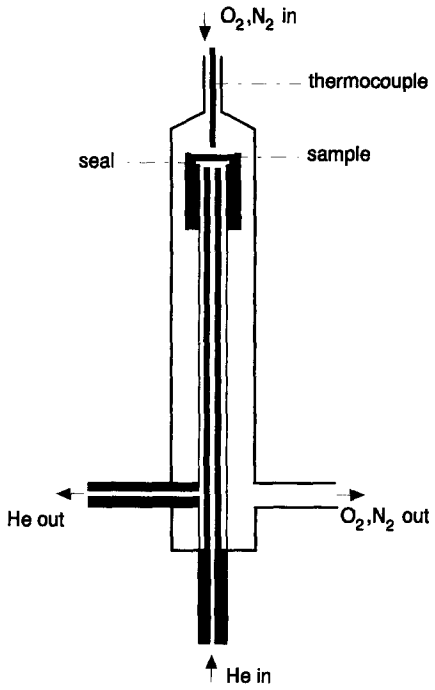

Fig. 4. Schematic diagram of the permeation reactor.

thickness were cut from the sintered disks and polished with 1000 MESH SiC. All results reported here refer to 1.0 mm thick membranes unless stated otherwise. The membrane densities exceed 92% of theoretical in all cases.

3.2. Oxygen permeation measurements

The measurements were performed in a quartz reactor with a reactor volume of approximately 3 ml, schematically shown in Fig. 4. 1.0 mm thick Supremax glass rings (Schott Nederland B.V.) were used to seal the membrane into the quartz reactor at 1310–1330 K in stagnant air. Prior to sealing, the cylindrical sides of the membrane were painted with Supremax-based paint. Before data were taken, the permeate sides of the membranes were treated in a CO-containing atmosphere. The reader is referred to the next section for details.

He (4.6N) was supplied to the permeate side of the membrane and the oxygen partial pressure in this compartment was varied by adjusting the total flow rate, under the assumption of ideal gas mixing. The oxygen partial pressure at the feed side could be varied between 0.01 and 1.0 bar by admixing of air, N_2 and O_2. Unless stated otherwise, all results reported here refer to measurements where air was supplied. The oxygen partial pressures of the retentate and permeate streams were continuously measured by YSZ-based oxygen sensors [37]. Analysis of the composition of the effluent stream was performed by a Varian 3300 gaschromatograph containing a molecular sieve 13X, which was coupled to a LDC/Milton Roy CL-10 integrator. All gas flows were controlled by Brooks 5800 mass flow controllers and the gas flow at the permeate side of the membrane was measured by a Brooks Volumeter. The oxygen flux was calculated from

$$J_{O_2} = \frac{1}{G} \cdot \frac{F c_{O_2}^{\text{permeate}}}{A}, \tag{21}$$

where F is the flow rate at the outlet of the reactor ($m^3\ s^{-1}$ (STP)), $c_{O_2}^{\text{permeate}}$ the oxygen concentration in the effluent stream (mol m^{-3}) and A the geometric surface area at the He-side of the membrane (m^2). G is a dimensionless factor that corrects for the effect of non-axial diffusion, which occurs due to the fact that the surfaces exposed to air and He have different surface areas. See Appendix for further details on the calculation of G.

The gas tightness of membrane and seal was checked by GC detection of N_2 in the effluent stream. The contribution of molecular oxygen to the total oxygen flux through leakages was in all cases below 1%. All measured fluxes were corrected for this contribution.

4. Results and discussion

4.1. Pretreatment

Upon sealing, the ambient of one of the membrane sides is changed from high (air) to low (He) oxygen partial pressure. Therefore the membrane nonstoichiometry will adapt to the newly applied gradient by loosing oxygen. The observed time-dependent oxygen flux will therefore consist of two contributions. The first is the time-independent, steady-state contribution; the second is a time-depen-

dent contribution due to the loss of lattice oxygen. The second contribution will finally disappear, so that it is expected to observe a steadily decreasing flux after sealing. In contrast, it was observed that after the sealing procedure was performed and the flow rates were set to fixed values, the oxygen flux tended to increase for long periods of time at 1273 K. This indicates a surface effect.

The stabilization of the oxygen flux was also found to be dependent on the level of Sr-doping. Lower Sr-concentrations resulted in longer stabilization times. An example is $La_{0.9}Sr_{0.1}FeO_{3-\delta}$, where the oxygen flux increased 50% during the first week after sealing. However, the flux had still only reached half of its final value.

The stabilization times differed from sample to sample, even for those with equal Sr-content. Some representative results are shown in Fig. 5. For $x = 0.4$, steady-state permeation is reached after 30 h. For $x = 0.2$, only a 20% increase is seen during the same period of time. Fig. 5 also shows the effect of a treatment of the He-side of the membrane in a 0.2 bar CO-containing atmosphere for $x = 0.3$. After treatment, the oxygen flux has increased significantly and restores quickly to a steady-state value after evacuation of all CO. Similar results were obtained for all other compositions. Treatments of 1.5–3 h were in all cases sufficient for the oxygen flux to increase significantly and further treatment did not result in any further increase of the flux. It should be noted that only the side of the membrane that is normally exposed to He was exposed to the He, CO,

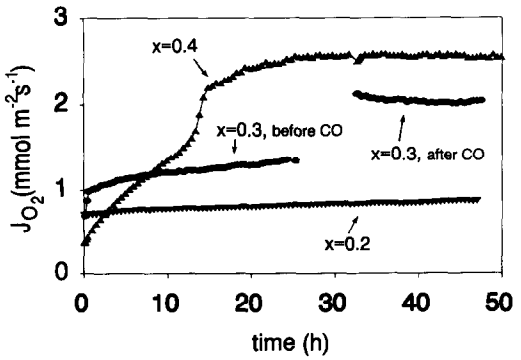

Fig. 5. Oxygen flux as a function of time after sealing at 1273 K for $x = 0.2$–0.4. $x = 0.2$: $F_{He} = 46.8$ ml/min (STP); $x = 0.3$: $F_{He} = 69.3$ ml/min (STP); $x = 0.4$: $F_{He} = 30.1$ ml/min (STP).

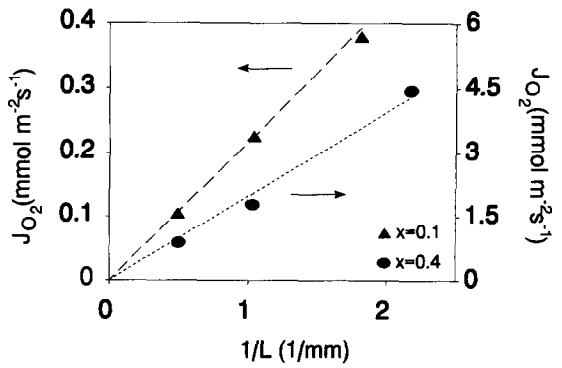

Fig. 6. Membrane thickness dependence of oxygen fluxes for $x = 0.1$ and $x = 0.4$ at 1273 K. Oxygen partial pressures at permeate side are $P_{O_2} = 10^{-3}$ bar ($x = 0.1$) and $P_{O_2} = 10^{-1.7}$ bar ($x = 0.4$).

CO_2 mixture. This indicates that the oxygen flux is initially limited by a surface exchange process at the permeate side of the membrane. All further results reported here apply to measurements that were performed after treatment in a CO-containing atmosphere. The nature of the effect of CO pretreatment will be reported elsewhere [30]. Possibly its main effect is that of an enlargement of the area on which oxygen exchange occurs.

4.2. Thickness dependence

The results of thickness dependence measurements for $x = 0.1$ and $x = 0.4$ are given in Fig. 6. It is clearly seen that the oxygen flux is inversely proportional to the membrane thickness for both compositions, in agreement with Eq. (15). These results strongly indicate an overall transport limitation by bulk diffusion.

The characteristic thicknesses L_c, shown in Table 1, suggest that in the membrane thickness range investigated here, an influence of the limiting role of surface exchange kinetics on oxygen permeation should be observed. In contrast, the experiments show a purely bulk-controlled permeation rate. As was already stated in the introduction, the characteristic thickness is not an intrinsic materials property. However, changing conditions affects the characteristic thickness by much less than an order of magnitude. The deviation between the predicted values and the observed bulk behaviour may be explained if it is

considered that the oxygen fluxes reported here were calculated by normalizing with respect to the geometric surface areas (A_g). The real surface area A_r may be several factors larger. This may imply that surface exchange can occur on a much larger area than the geometrical one. Hence the characteristic thickness for the membrane systems investigated here may be a factor of A_g/A_r smaller than as determined from Eq. (1).

4.3. Oxygen partial pressure dependence

Another indication for a bulk-controlled flux is obtained from the oxygen partial pressure dependence of the oxygen flux. Regardless of the nature of the rate-limiting transport process, the oxygen flux can be related to the oxygen partial pressure by the empirical equation

$$J_{O_2} = \alpha P_{O_2}^n + \beta, \qquad (22)$$

α, β and n are constants. Their values may be obtained by least-squares fitting of results of experiments in which the oxygen partial pressure is varied on one side of the membrane. In the case of a bulk diffusion-controlled flux, the value of n should be close to that of $\langle n \rangle$ in Eq. (20), if the limits of integration are set properly in the latter formula.

Fig. 7 shows fluxes from experiments in which the oxygen partial pressure at the feed side was varied between 10^{-2} and 1 bar at 1273 K. Least-squares fitting of the experimental values to Eq. (22) results in values of n_{expt} as shown in Table 4. The corresponding theoretical values $\langle n \rangle$ are also given. Since no data were available for $x = 0.2$ and $x = 0.3$ from literature, the data for $x = 0.25$ were used for modelling in these two cases (except for the value of x). There is a fair agreement between the experimental and theoretical dependencies. In the partial pressure range considered here, $\sigma_{el} \gg \sigma_{ion}$. Thus, taking Eq. (19) into account, the comparison between n_{expt} and $\langle n \rangle$ mainly shows that the experimental results are in agreement with the nonstoichiometry model of Mizusaki et al. [16]. In Fig. 8, the absolute values of the fluxes of $x = 0.1$ are compared with a model calculation, based on literature data. As can be seen, the model calculation predicts higher fluxes than were determined experimentally. If we assume that the deviation between the model calculation and the experimental results is mainly caused by the error in the reported vacancy diffusion coefficient, the experimental results can be fitted by adjusting the value of

Table 4
Experimental $n_{expt.}$ (Eq. (22)) and theoretical values $\langle n \rangle$ (Eq. (20)) for the power dependence of the oxygen flux on the oxygen partial pressure at 1273 K.

x	$n_{expt.}$	$\langle n \rangle$
0.1	−0.39	−0.42
0.2	−0.24	−0.20
0.3	−0.17	−0.16
0.4	−0.09	−0.12

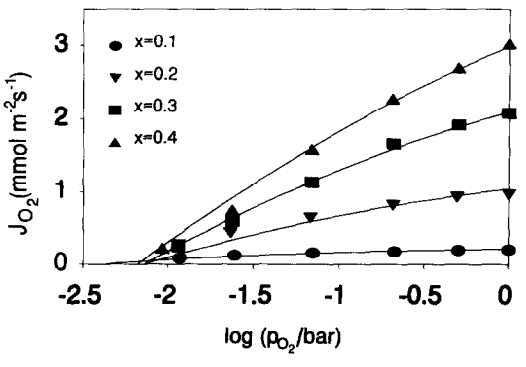

Fig. 7. Fluxes with varying oxygen partial pressure at the feed side at 1273 K. Permeate side oxygen partial pressures are 3.8×10^{-3} bar ($x = 0.1$), 7.3×10^{-3} bar ($x = 0.2, 0.3$) and 6.8×10^{-3} bar ($x = 0.4$). Drawn lines indicate best fit.

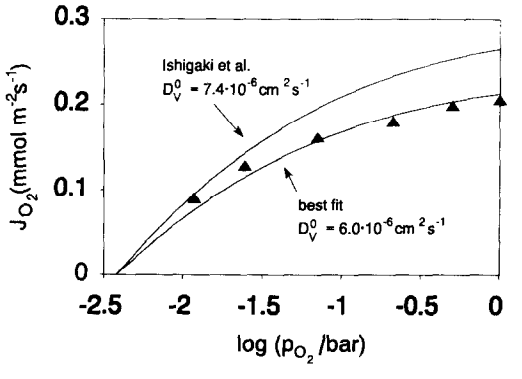

Fig. 8. Comparison between experimental values of feed side dependence of $x = 0.1$ and Wagner theory at 1273 K. Best fit to the experimental data, as described in the text, and curve calculated from literature data (Ref. [29]) are shown.

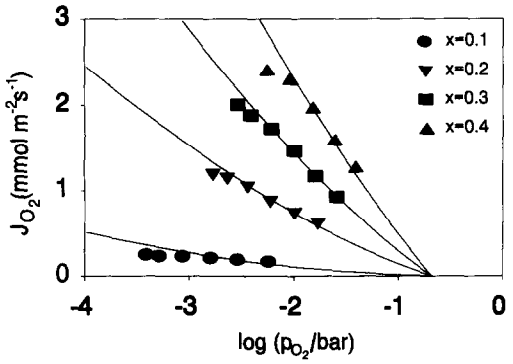

Fig. 9. Fluxes with varying oxygen partial pressure at the permeate side at 1273 K. Drawn lines indicate least-squares fits to Wagner equation as described in the text.

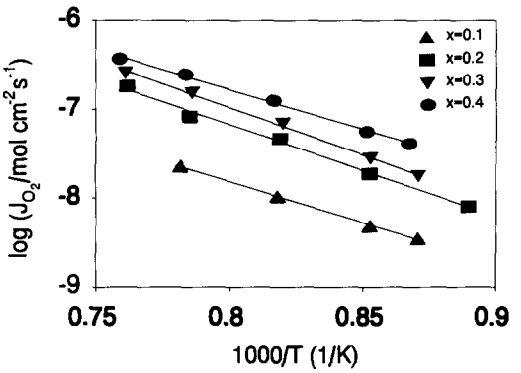

Fig. 10. Temperature dependencies between 1123–1323 K for $x = 0.1$–0.4 in a fixed gradient (Table 6). Since the measurement for $x = 0.4$ was obtained on a 2.01 mm thick sample, the experimental values and least-squares fit for $x = 0.4$ have an offset of $^{10}\log 2$ for reasons of consistency.

D_V^0 only. This adjustment will not influence the calculated $\langle n \rangle$-values. Attributing the difference between model and experimental data to the nonstoichiometry model is less likely, because fitting the fluxes by changing the thermodynamic quantities would involve very large adjustments.

Least-squares refinement for all compositions leads to values for D_V^0 that are 20–60% lower than as reported by Ishigaki et al. [29]. Fig. 7 shows the curves obtained with the best fits. The same procedure was applied to the permeate-side partial pressure dependence of the flux. The experimental values and the fitted curves are shown in Fig. 9. The values of D_V^0, fitted independently from both dependencies, are in close agreement. The results for both types of fits are given in Table 5. The largest deviation is found for $x = 0.4$, being equal to 20%.

Table 5
D_V^0 values at 1273 K determined from two least-squares fits of oxygen permeation experiments to Wagner model. Conditions are described in the text

x	D_V^0 (10^{-6} cm^2 s^{-1})	D_V^0 (10^{-6} cm^2 s^{-1})
	high P_{O_2}-side	low P_{O_2}-side
0.1	5.98	5.32
0.2	7.84	7.58
0.3	8.16	7.96
0.4	7.77	9.34

4.4. Temperature dependence

The activation energies were determined between 1123–1323 K. If we assume that $\sigma_{amb} \approx \sigma_{ion}$, then it can be seen from Eqs. (12) and (15) that the apparent activation energy of oxygen semi-permeability is given by

$$E_{act}(J_{O_2}) = E_{act}(D_V) + E_{act}(\delta). \quad (23)$$

Since Fig. 3 showed the activation energy for oxygen vacancy formation to depend strongly on the oxygen partial pressure, the activation energy for oxygen permeation will be dependent on the gradient. Therefore, oxygen permeation measurements were performed as a function of temperature with a fixed

Table 6
Experimental activation energies of the oxygen flux in a fixed gradient in the temperature range 1123–1323 K. P_{O_2} indicates oxygen partial pressure at the permeate side. Calculated activation energies for oxygen vacancy formation in corresponding gradient are also shown

x	P_{O_2} (bar)	E_{act} (J) (kJ mol^{-1})	E_{act} (δ) (kJ mol^{-1})
0.1	1.0×10^{-3}	178 ± 7	65
0.2	2.5×10^{-3}	199 ± 18	38
0.3	5.0×10^{-3}	206 ± 12	32
0.4 [a]	3.0×10^{-3}	173 ± 11	21

[a] Obtained on a 2.01 mm thick membrane.

oxygen partial pressure gradient for each composition independently. The Arrhenius plots are shown in Fig. 10. The corresponding activation energies and experimental conditions are shown in Table 6. All values are in the range of 170–210 kJ/mol. Also shown in Table 6 are the activation energies of oxygen vacancy formation in the same gradient, as calculated from the nonstoichiometry model. Accordingly, in view of Eq. (23), the activation energies of the vacancy diffusion coefficient will have values in the range of 113–175 kJ/mol. Ishigaki et al. [29] reported activation energies for the vacancy diffusion coefficient in the range of 75–85 kJ/mol at an oxygen partial pressure of 0.065 bar. Since the vacancy diffusion coefficient cannot be expected to depend strongly on the oxygen partial pressure, these results do not seem to be in agreement. Possibly, an explanation can be found from the fact that the aforementioned study of Ishigaki et al. was performed on single crystals, in contrast to the polycrystalline membranes used here.

5. Conclusions

It was shown that the oxygen semi-permeability of $La_{1-x}Sr_xFeO_{3-\delta}$ ($x = 0.1$–0.4) membranes can be increased significantly by exposure of the membrane lower partial pressure side in CO. The oxygen fluxes through pretreated membranes of 0.5–2.0 mm thickness can be described properly in terms of a bulk diffusion-limited permeation behaviour. Assuming a point defect model, qualitatively good agreement was found with the experimental data. Quantitative agreement was obtained by adjustment of the vacancy diffusion coefficients D_V^0 in the model. The D_V^0 values were virtually independent of composition and were in the range 5.3–9.3×10^{-6} cm^2 s^{-1}. With respect to the differences found between the vacancy diffusion coefficients reported here and those reported by Ishigaki et al. [28,29], it may be concluded that the agreement is fair, since they do not differ by more than a factor of 2.5. A stronger deviation between both series of results is found in the trends upon changing the Sr concentration. Both series of diffusion coefficients are shown in Fig. 11. The vacancy diffusion coefficients found in this study slightly increase with x. A larger dependence is found in Ishigaki's study.

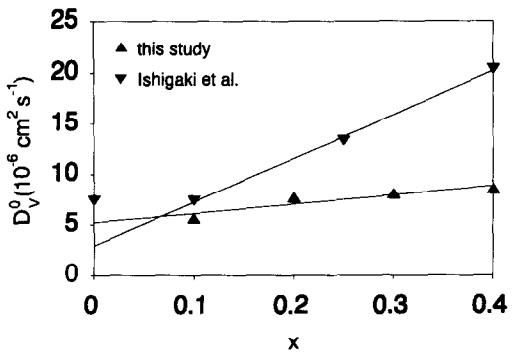

Fig. 11. Comparison of vacancy diffusion coefficients with data from Ref. [29].

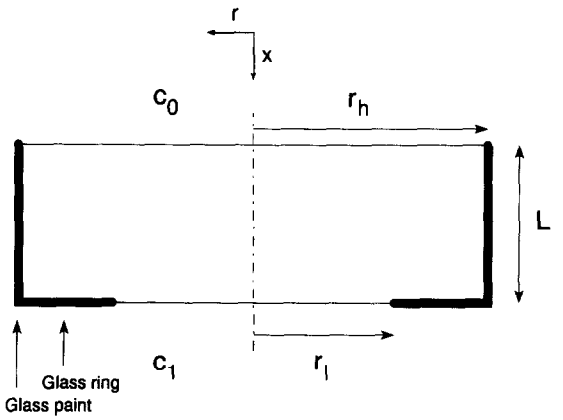

Fig. 12. Schematic diagram of membrane geometry. Thick lines indicate insulating boundaries. Gas phase oxygen concentrations are indicated as c_0 and c_1.

The activation energies of oxygen permeation were found to be in the range of 170–210 kJ/mol and were much larger than is expected on the basis of literature data. We found no clear explanation for this discrepancy.

Appendix

Due to the applied method of sealing, the membrane side exposed to He has a smaller surface area than the side exposed to O_2/N_2. This sealing effect is schematically depicted in Fig. 12. As a result, the oxygen flux has a non-zero radial component. Since

the measured oxygen flux is normalized with respect to the He-side surface area, the axial flux is overestimated. A factor G can be calculated to correct for this effect and in order to obtain the one-dimensional, axial oxygen flux.

The basic equation to be solved is the steady-state diffusion equation in cylindrical coordinates

$$D\left(\frac{\partial^2 c}{\partial x^2}+\frac{\partial^2 c}{\partial r^2}+\frac{1}{r}\frac{\partial c}{\partial r}\right)=0, \tag{24}$$

where D ($cm^2\ s^{-1}$) is the diffusion coefficient (assumed isotropically) and c the oxygen concentration ($mol\ m^{-3}$). The boundary conditions are

$$c(x=0)=c_0, \tag{25}$$

$$c(x=L,\ r\leqslant r_i)=c_1, \tag{26}$$

for the gas/solid interfaces,

$$\left(\frac{\partial c}{\partial r}\right)_{r=r_h}=0, \tag{27}$$

$$\left(\frac{\partial c}{\partial x}\right)_{x=L,r>r_i}=0 \tag{28}$$

for the insulating boundaries, and

$$\left(\frac{\partial c}{\partial r}\right)_{r=0}=0 \tag{29}$$

for the central axis. This set of equations can be solved numerically or analytically [38] under certain assumptions. This will finally result in an oxygen flux J_r. Dividing this flux by the calculated one-dimensional flux J_a will yield G. For the membranes used in this study, $r_i = 4.5$ mm and $r_h = 6$ mm. The correction factors used here were calculated by a numerical procedure and were found to be equal to 1.12, 1.21 and 1.38 for membranes of 0.5, 1.0 and 2.0 mm thickness, respectively.

Acknowledgements

The support of the Commission of the European Communities in the framework of the Joule programme, sub-programme Energy from Fossil Resources, Hydrocarbons, is gratefully acknowledged. M.H.R. Lankhorst is acknowledged for providing the numerical procedure for the calculation of the geometric correction factor.

References

[1] H.U. Anderson, Solid State Ionics 52 (1992) 33.
[2] P.J. Gellings and H.J.M. Bouwmeester, Catal. Today 12 (1992) 1.
[3] A.G. Dixon, W.R. Moser and Y.H. Ma, Ind. Eng. Chem. Res. 33 (1994) 3015.
[4] S. Dou, C.R. Masson and P.D. Pacey, J. Electrochem. Soc. 132 (1985) 1843.
[5] Y. Nigara and B. Cales, Bull. Chem. Soc. Japan 59 (1986) 1997.
[6] G.Z. Cao, X.Q. Liu, H.W. Brinkman, K.J. de Vries and A.J. Burggraaf in: Science and Technology of Zirconia V, ed. S.P.S. Badwal, M.J. Bannister and R.J.H. Hannink, (Technomic Publishing, Pennsylvania-Basel, 1993) p. 577.
[7] H.J.M. Bouwmeester, H. Kruidhof, A.J. Burggraaf and P.J. Gellings, Solid State Ionics 53–56 (1992) 460.
[8] Y. Teraoka, T. Nobunaga and N. Yamazoe, Chem. Lett. (1988) 503.
[9] R.H.E. van Doorn, H. Kruidhof, H.J.M. Bouwmeester and A.J. Burggraaf, Proc. MRS Fall Meeting, Oct. 27–Nov. 2, Boston (MA), USA.
[10] N. Itoh, T. Kato, K. Uchida and K. Haraya, J. Membr. Sci. 92 (1994) 239.
[11] Y. Teraoka, T. Nobunaga, K. Okamoto, N. Miura and N. Yamazoe, Solid State Ionics 48 (1991) 207.
[12] T. Nakamura, G. Petzow and L.J. Gauckler, Mat. Res. Bull. 14 (1979) 649.
[13] A.N. Petrov, V.A. Cherepanov, O.F. Kononchuk and L. Ya. Gavrilova, J. Solid State Chem. 87 (1990) 69.
[14] H.J.M. Bouwmeester, H. Kruidhof and A.J. Burggraaf, Solid State Ionics 72 (1994) 185.
[15] H. Schmalzried, Solid State Reactions, 2nd Ed. (Verlag Chemie, Weinheim, 1981).
[16] J. Mizusaki, M. Yoshihiro, S. Yamauchi and K. Fueki, J. Solid State Chem. 58 (1985) 257.
[17] F.A. Kröger, The Chemistry of Imperfect Crystals (North-Holland, Amsterdam, 1964).
[18] J. Mizusaki, M. Yoshihiro, S. Yamauchi and K. Fueki, J. Solid State Chem. 67 (1987) 1.
[19] C.N.R. Rao, J. Gopalakrishnan and K. Vidyasagar, Ind. J. Chem. 23A (1984) 265.
[20] Y. Takeda, K. Kanno, T. Takada, O. Yamamoto, M. Takano, N. Nakayama and Y. Bando, J. Solid State Chem. 63 (1986) 237.
[21] P.D. Battle, T.C. Gibb and S. Nixon, J. Solid State Chem. 79 (1989) 75.
[22] J.-C. Grenier, N. Ea, M. Puchard and P. Hagenmuller, J. Solid State Chem. 58 (1985) 243.
[23] M.A. Alario-Franco, M.J.R. Henche, M. Vallet, J.M.G. Calbet, J.-C. Grenier, A. Wittiaux and P. Hagenmuller, J. Solid State Chem. 46 (1983) 23.

[24] J.M. González-Calbet, M. Vallet-Regi and M.A. Alario-Franco, Mat. Res. Bull. 18 (1983) 285.
[25] L. Fournès, Y. Potin, J.-C. Grenier, G. Demazeau and M. Pouchard, Solid State Commun. 62 (1987) 239.
[26] M. Takano, T. Okita, N. Nakayama, Y. Bando, Y. Takeda, O. Yamamoto and J.B. Goodenough, J. Solid State Chem. 73 (1988) 140.
[27] J.M. González-Calbet, M. Parras, M. Vallet-Regi and J.C. Grenier, J. Solid State Chem. 92 (1991) 110.
[28] T. Ishigaki, S. Yamauchi, J. Mizusaki, K. Fueki, H. Naito and T. Adachi, J. Solid State Chem. 55 (1984) 50.
[29] T. Ishigaki, S. Yamauchi, K. Kishio, J. Mizusaki and K. Fueki, J. Solid State Chem. 73 (1988) 179.
[30] J.E. ten Elshof, H.J.M. Bouwmeester and H. Verweij, to be published.
[31] J.B. Goodenough, Proc. Roy. Soc. London, A 393 (1984) 215.
[32] M.C. Kim, S.J. Park, H. Haneda, J. Tanaka, T. Mitsuhasi and S. Shirasaki, J. Mat. Sci. Lett. 9 (1990) 102.
[33] R.J.H. Voorhoeve, in: Advanced Materials in Catalysis, eds. J.J. Burton and R.L. Garten (Academic Press, New York, 1977) p. 129.
[34] J. Mizusaki, T. Sasamoto, W.R. Cannon and H.K. Bowen, J. Am. Ceram. Soc. 66 (1983) 247.
[35] S.E. Dann, D.B. Currie, M.T. Weller, M.F. Thomas and A.D. Al-Rawwas, J. Solid State Chem. 109 (1994) 134.
[36] B.A. van Hassel, T. Kawada, N. Sakai, H. Yokokawa, M. Dokiya and H.J.M. Bouwmeester, Solid State Ionics 66 (1993) 295.
[37] B.A. van Hassel, J.E. ten Elshof and H.J.M. Bouwmeester, Appl. Catal. A: General 119 (1994) 279.
[38] K.H. Keller and T.R. Stein, Math. Biosci. 1 (1967) 421.